Geomechanics and Engineering, *Vol. 7*, *No. 4* (*2014*) *403-430*
DOI: http://dx.doi.org/10.12989/gae.2014.7.4.403

Hydraulic fracture initiation pressure of anisotropic shale gas reservoirs

Haiyan Zhu [*1], Jianchun Guo [1a], Xing Zhao [1], Qianli Lu [1], Bo Luo [1] and Yong-cun Feng [2]

[1] *State Key Laboratory of Oil & Gas Reservoir Geology and Exploitation, Southwest Petroleum University, Chengdu 610500, China*
[2] *Department of Petroleum and Geosystems Engineering, The University of Texas at Austin, Austin, TX, 78712, USA*

(*Received December 12, 2013, Revised June 09, 2014, Accepted June 25, 2014*)

Abstract. Shale gas formations exhibit strong mechanical and strength anisotropies. Thus, it is necessary to study the effect of anisotropy on the hydraulic fracture initiation pressure. The calculation model for the in-situ stress of the bedding formation is improved according to the effective stress theory. An analytical model of the stresses around wellbore in shale gas reservoirs, in consideration of stratum dip direction, dip angle, and in-situ stress azimuth, has been built. Besides, this work established a calculation model for the stress around the perforation holes. In combination with the tensile failure criterion, a prediction model for the hydraulic fracture initiation pressure in the shale gas reservoirs is put forward. The error between the prediction result and the measured value for the shale gas reservoir in the southern Sichuan Province is only 3.5%. Specifically, effects of factors including elasticity modulus, Poisson's ratio, in-situ stress ratio, tensile strength, perforation angle (the angle between perforation direction and the maximum principal stress) of anisotropic formations on hydraulic fracture initiation pressure have been investigated. The perforation angle has the largest effect on the fracture initiation pressure, followed by the in-situ stress ratio, ratio of tensile strength to pore pressure, and the anisotropy ratio of elasticity moduli as the last. The effect of the anisotropy ratio of the Poisson's ratio on the fracture initiation pressure can be ignored. This study provides a reference for the hydraulic fracturing design in shale gas wells.

Keywords: shale gas; hydraulic fracturing; initiation pressure; bedding formation; prediction model

1. Introduction

Nowadays, it has been difficult for conventional resources to meet the oil and gas demand and shale reservoirs have been extensively arousing the public attention as a typical unconventional resource (Bowker 2003). Compared to conventional reservoirs, the porosity and permeability of shale gas reservoirs are very low, with gas being stored in both adsorbed and free state in the organic rich rock. Based on the estimation of the US Energy Information Administration (EIA), the geological reserve of shale gas is up to 623 trillion cubic meters and the recoverable reserve is

*Corresponding author, Ph.D., E-mail: zhuhaiyan040129@163.com
[a] Professor, E-mail: guojianchun@vip.163.com

http://www.techno-press.org/?journal=gae&subpage=7 ISSN: 2005-307X (Print), 2092-6219 (Online)

up to 163 trillion cubic meters, indicating a prosperous development prospect (EIA 2011).

Generally, all shale gas reservoirs need fracturing treatment to achieve commercial production due to its ultra-low permeability and various gas occurrence states, except that a minority with existing fracture-developed zones may have a high natural production capacity (Mathews *et al*. 2007). The stress around the shale gas well also differs from that of the homogeneous sandstone reservoir due to the severe anisotropy. Lekhnitskii (1981) established the mechanical foundation of anisotropic formations. Amadei (1983) calculated the stress distributions around various types of wells in formations with different magnitude of anisotropy based on the plane strain assumption. The analytical solutions derived by Amadei (1983), including three coordination systems (in-situ stress, well-hole, and stratum), are very complex and seldom applied. Aadnøy and høgskole (1987) computed the stress field around the wellbore in transverse isotropic media, and set up the collapse pressure model and fracture initiation pressure model of the borehole wall in anisotropic strata utilizing the anisotropic elastomer model proposed by Lekhnitskii (1981). He suggested that the zero tensile strength and the tensile strength of rock without cracks should be separately substituted into the fracture initiation pressure models to solve for the upper and lower bounds of the fracture initiation pressure of the borehole wall. Ong (1994) added the non-linear and porous media effects into the model of Aadnøy and høgskole (1987). Later, Ong and Roegiers (1995) presented the fracture initiation model for directional openhole wells in anisotropic formations. Suarez-Rivera *et al*. (2009) predicted the fracture initiation pressure of the wall of the shale well using anisotropic failure criterion given by Pariseau (1968). Suarez-Rivera *et al*. (2006) and Khan *et al*. (2011) calculated the stress distribution around the horizontal well in anisotropic formations and studied the effect of anisotropy factors on shale fracture initiation pressure based on the failure criterion proposed by Jaeger and Cook (1979).

In previous studies, some scholars have established or improved the models of fracture initiation pressure for the directional wells in bedding formations, but few scholars have studied the prediction model for that of the perforated well. These studies focused on the anisotropy of the shale strength and all of the in-situ stress is treated as occurred in a homogeneous isotropic body. Apparently, this is unreasonable for the transverse isotropic body of shale and the conventional model for in-situ stress is no longer applicable to the shale formations due to the difference between the elastic parameters perpendicular to and parallel to the direction of bedding plane. In response to these restrictions, Wang *et al*. (1999) proposed a model for transverse isotropic body, which improved the in-situ stress calculation in bedding formation, by taking the effective stress and stratum dipping into consideration. In this paper, a hydraulic fracture initiation pressure model was established upon the calculation of the stress around the perforation in shale gas wells. Their case study of the model in the shale gas reservoir in southern Sichuan Province further verified the effect of the shale strength parameters and in-situ stress on the fracture initiation pressure.

2. Prediction model of fracture initiation pressure in anisotropic shale

2.1 Calculation model for in-situ stress in bedding formation

Currently, the quantitative studies mostly deal with homogeneous and isotropic formations, where the prediction models for in-situ stress, such as Terzaghi model, Anderson model and "Six-Five" model and "Seven-Five" model proposed by Huang and Zhuang (1986), are widely-used. However, the shale formation is a type of transverse isotropic body and it is obviously unreasonable to apply the homogeneous model to evaluate the wellbore stability

problem. Thiercelin and Plumb (1994) discussed the calculation model for the linear elastic in-situ stress of transverse isotropic strata considering the effects of overlying stratum pressure and tectonic stress. Prioul *et al*. (2011) gave a theoretical expression regarding the effects of stratum uplift, pore pressure, and tectonic pressure levels on the horizontal in-situ stress. Based on the structural mechanical principles of the composite material, Wang and Li (1999) proposed a calculation model for in-situ stress in transverse isotropic strata under different bedding occurrences.

It is opined that, excluding any abnormal high pressure caused by tectonic movement, the tectonic movement and shale anisotropy only affect the frame stress but will not affect the pore pressure. Besides, according to the effective stress theory of porous media, and referring to Wang's and Huang's Models, the above two factors and the Biot's coefficient are selected as the weight values of the effective stress and pore pressure, respectively. Then stratum dipping is integrated to calculate the horizontal principal stress

$$\begin{cases} \sigma_H = \left[\dfrac{v_v E}{(1-v)E_v} + A\right](\sigma_V - \alpha P_p)\cos\beta_r + (\sigma_V - \alpha P_p)\sin\beta_r \cos(\alpha_r - \omega_o) + \alpha P_p \\ \sigma_h = \left[\dfrac{v_v E}{(1-v)E_v} + B\right](\sigma_V - \alpha P_p)\cos\beta_r + (\sigma_V - \alpha P_p)\sin\beta_r \sin(\alpha_r - \omega_o) + \alpha P_p \end{cases} \tag{1}$$

where, A and B are tectonic stress coefficients, E, E_v, v and v_v are elastic parameters of the transverse isotropic body, α_r and β_r are the dip direction and dip angle of the bedding plane, σ_V is the vertical stress, α is the effective stress coefficient, P_p is the pore pressure, and w_o is the maximum horizontal principal stress orientation.

2.2 Analytical model for stresses around wellbore in anisotropic shale reservoirs

In general, a horizontal section or high-inclination section is drilled in the shale formation and the calculation model for stresses around wellbore is shown in Fig. 1. Fig. 2 presents the

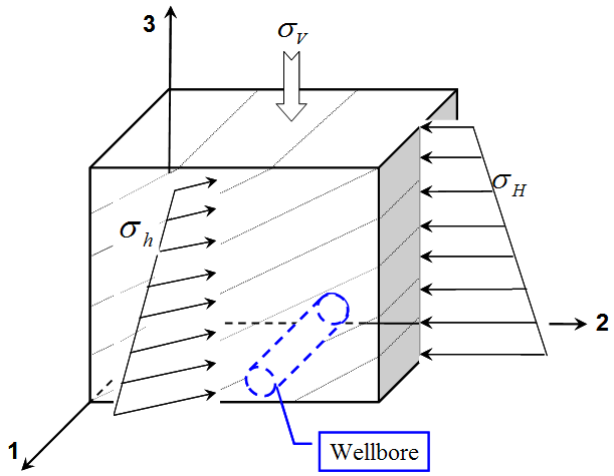

Fig. 1 Calculation model for stresses around wellbore in shale formation

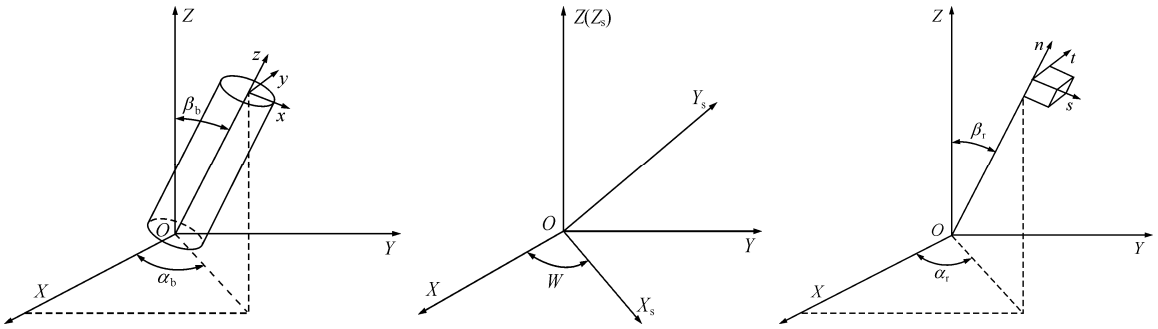

(a) Wellbore coordinate system (b) In-situ stress coordinate system (c) Bedding plane coordinate system

Fig. 2 Corresponding relationship between local coordinate system and geomagnetic coordinate system

coordinate transform relationship in the stresses analysis of shale borehole wall: (1) geomagnetic coordinate system [*X Y Z*] (*X*, *Y* and *Z* correspond to the due east, due north, and the magneticdipole directions respectively); (2) well coordinate system [*x y z*], β_b is the well deviation angle and α_b is the well azimuth angle; (3) in-situ stress system [X_s Y_s Z_s], X_s, Y_s and Z_s correspond to the three primary stresses, σ_H, σ_h and σ_v; and the orientation of maximum horizontal in-situ stress is *W*; (4) bedding plane coordinate system [*s t n*].

Within the in-situ stress coordinate system, the original stress state is

$$[\sigma]=\begin{bmatrix}\sigma_H & 0 & 0\\ 0 & \sigma_h & 0\\ 0 & 0 & \sigma_v\end{bmatrix} \tag{2}$$

Based on the transformation relations among coordinate systems, the transformation matrix between the in-situ stress coordinate system and the well coordinate system is

$$[L]=\begin{bmatrix}\cos\beta_b\cos\alpha' & \cos\beta_b\sin\alpha' & -\sin\beta_b\\ -\sin\alpha' & \cos\alpha' & 0\\ \sin\beta_b\cos\alpha' & \sin\beta_b\sin\alpha' & \cos\beta_b\end{bmatrix} \tag{3}$$

where, $\alpha' = W - \alpha_b$

In the well coordinate system, the initial stress state is

$$\begin{bmatrix}\sigma_{xx} & \sigma_{xy} & \sigma_{xz}\\ \sigma_{yx} & \sigma_{yy} & \sigma_{yz}\\ \sigma_{zx} & \sigma_{zy} & \sigma_{zz}\end{bmatrix}=[L]\begin{bmatrix}\sigma_H & & \\ & \sigma_h & \\ & & \sigma_v\end{bmatrix}[L]^T \tag{4}$$

Without considering the gravity, the stresses around wellbore in the rectangular coordinate system of well should meet the equilibrium differential equation

$$\begin{cases} \dfrac{\partial \sigma_x}{\partial x} + \dfrac{\partial \tau_{yx}}{\partial y} + \dfrac{\partial \tau_{xz}}{\partial z} = 0 \\ \dfrac{\partial \tau_{xy}}{\partial x} + \dfrac{\partial \sigma_y}{\partial y} + \dfrac{\partial \tau_{yz}}{\partial z} = 0 \\ \dfrac{\partial \tau_{xz}}{\partial x} + \dfrac{\partial \tau_{yz}}{\partial y} + \dfrac{\partial \sigma_z}{\partial z} = 0 \end{cases} \tag{5}$$

The strain component is independent of z in accordance with the plane strain principles in the broad sense. Then, the consistent equation can be expressed as

$$\begin{cases} \dfrac{\partial^2 \varepsilon_x}{\partial y^2} + \dfrac{\partial^2 \varepsilon_y}{\partial x^2} = \dfrac{\partial^2 \gamma_{xy}}{\partial x \partial y} \\ \dfrac{\partial \gamma_{xz}}{\partial y} - \dfrac{\partial \gamma_{yz}}{\partial x} = 0 \\ \dfrac{\partial^2 \varepsilon_z}{\partial y^2} = \dfrac{\partial^2 \varepsilon_z}{\partial x^2} = \dfrac{\partial^2 \varepsilon_z}{\partial x \partial y} = 0 \end{cases} \tag{6}$$

Under the small deformation conditions, the geometric equation is

$$\varepsilon_{ij} = \frac{1}{2}\left(u_{i,j} + u_{j,i}\right) \tag{7}$$

where, is $\varepsilon_{i,j}$ the strain component of the stratum, $u_{i,j}$ and $u_{j,i}$ are displacement components, respectively.

Based on the Biot effective stress theory, the following can be obtained (Zhu *et al*. 2013a)

$$\sigma'_{ij} = \sigma_{ij} - \alpha P_p \delta_{ij} \tag{8}$$

where, σ'_{ij} is the effective stress component, and δ_{ij} is the Kronecker symbol (when $i = j$, $\delta_{ij} = 1$; otherwise, $\delta_{ij} = 0$).

Shale is characteristic of transverse isotropy and its constitutive equation can be expressed with the modified Hooke's law (Sayers 2005)

$$\sigma'_{ij} = \mathbf{D}_{\mathrm{T}} \varepsilon_{ij} \tag{9}$$

$$\mathbf{D}_{\mathrm{T}}=\begin{pmatrix} \frac{1}{E_h} & -\frac{v_{hh}}{E_h} & -\frac{v_{vh}}{E_v} & & & \\ -\frac{v_{hh}}{E_h} & \frac{1}{E_h} & -\frac{v_{vh}}{E_v} & & & \\ -\frac{v_{vh}}{E_h} & -\frac{v_{vh}}{E_h} & \frac{1}{E_v} & & & \\ & & & \frac{1}{G_{vh}} & & \\ & & & & \frac{1}{G_{vh}} & \\ & & & & & \frac{2(1+v_{hh})}{E_h} \end{pmatrix} \tag{10}$$

where, E_v is the elasticity modulus in the perpendicular direction; E_h is the elasticity modulus in the horizontal direction; v_v is the Poisson's ratio of the horizontal strain when vertical strain is applied; v_h is the Poisson's ratio of the horizontal strain when horizontal normal strain is applied; G_v is the shear modulus in the vertical plane; G_h is the shear modulus in the horizontal plane. Only five of the six elastic parameters above are independent (E_v, E_h, v_v, and G_v), as can either be obtained by a core mechanical test directly or a acoustic wave test indirectly (Sinha *et al*. 2006, Walsh *et al*. 2007). It is isotropic in the horizontal direction, G_h and G_v are

$$\frac{1}{G_h}=\frac{2(1+v_h)}{E_h} \tag{11}$$

$$\frac{1}{G_h}=\frac{1}{E_h}+\frac{1}{E_v}+2\frac{v_v}{E_v} \tag{12}$$

The elasticity matrix given above is defined in the local coordinate system in the bedding plane, whereas in the wellbore stability analysis, the stress and deformation occur under the well coordinate system. Therefore, the elasticity matrix under the bedding plane coordinate system needs to be transformed into the well coordinate system.

Based on the transformation relationship among coordinate systems given in Fig. 1, the elasticity matrix **D** under the well coordinate system is

$$\mathbf{D}=\mathbf{q}\mathbf{D}_{\mathrm{T}}\mathbf{q} \tag{13}$$

$$\mathbf{q}=\begin{bmatrix} \cos^2\gamma & 0 & \sin^2\gamma & 0 & -2\sin\gamma\cos\gamma & 0 \\ 0 & 1 & 0 & 0 & 0 & 0 \\ \sin^2\gamma & 0 & \cos^2\gamma & 0 & 2\sin\gamma\cos\gamma & 0 \\ 0 & 0 & 0 & \cos\gamma & 0 & \sin\gamma \\ \sin\gamma\cos\gamma & 0 & -\sin\gamma\cos\gamma & 0 & \cos^2\gamma-\sin^2\gamma & 0 \\ 0 & 0 & 0 & -\sin\gamma & 0 & \cos\gamma \end{bmatrix} \tag{14}$$

where, γ is the included angle between the normal direction of the bedding plane and the well axis.

Based on the solutions to the anisotropic plane problem by Lekhnitskii (1981), Amadei (1983), Aadnøy and høgskole (1987) and Ong (1994), the analytical model for the stresses around wellbore in the bedding shale reservoir is obtained by superimposing the far field in-situ stress and the stress arising from the boundary conditions of the well and borehole wall.

$$\begin{cases} \sigma_x = \sigma_{x,0} + 2\,\mathrm{Re}\left\{ \mu_1^2\varphi_1'(z_1) + \mu_2^2\varphi_2'(z_2) \right\} \\ \sigma_y = \sigma_{y,0} + 2\,\mathrm{Re}\left\{ \varphi_1'(z_1) + \varphi_2'(z_2) \right\} \\ \tau_{xy} = \tau_{xy,0} - 2\,\mathrm{Re}\left\{ \mu_1\varphi_1'(z_1) + \mu_2\varphi_2'(z_2) \right\} \\ \tau_{xz} = \tau_{xz,0} + 2\,\mathrm{Re}\left\{ \mu_3\varphi_3'(z_3) \right\} \\ \tau_{yz} = \tau_{yz,0} - 2\,\mathrm{Re}\left\{ \varphi_3'(z_3) \right\} \\ \sigma_z = \sigma_{z,0} - 2\,\mathrm{Re}\left\{ a_{31}\left[\mu_1^2\phi_1'(z_1) + \mu_2^2\phi_2'(z_2)\right] + a_{32}\left[\phi_1'(z_1) + \phi'(z_2)\right] \right\} \Big/ a_{33} \end{cases} \tag{15}$$

The expression of the variable z_k is: $z_k = x + \mu_k y$ (k = 1, 2, 3) and the analytical function ϕ_k (z_k) is determined by the boundary conditions. On the borehole wall $x = R\cos\theta$, $y = R\sin\theta$, according to the study by Lekhnistskii, the partial derivative of the analytical function around the borehole wall is (Ong 1994)

$$\left.\begin{aligned} \phi_1'(z_1) &= \frac{1}{2\Delta(\mu_1\cos\theta - \sin\theta)}(E'\mu_2 - D') \\ \phi_2'(z_2) &= \frac{1}{2\Delta(\mu_2\cos\theta - \sin\theta)}(D' - E'\mu_1) \\ \phi_3'(z_3) &= \frac{1}{2\Delta(\mu_3\cos\theta - \sin\theta)}(F'\mu_2 - \mu_1) \end{aligned}\right\} \tag{16}$$

where

$$\left.\begin{aligned} \Delta &= \mu_2 - \mu_1 \\ D' &= (P_w - \sigma_{x,0})\cos\theta - \tau_{xy,0}\sin\theta - i(P_w - \sigma_{x,0})\sin\theta - i\tau_{xy,0}\cos\theta \\ E' &= -(P_w - \sigma_{y,0})\sin\theta - \tau_{xy,0}\cos\theta - i(P_w - \sigma_{y,0})\cos\theta - i\tau_{xy,0}\sin\theta \\ F' &= -\tau_{xz,0}\cos\theta - \tau_{xz,0}\sin\theta + i\tau_{xz,0}\sin\theta - i\tau_{xz,0}\cos\theta \end{aligned}\right\} \tag{17}$$

where, σ_x, σ_y, σ_z, τ_{xy}, τ_{xz} and τ_{yz} are the components of the stresses around wellbore, MPa; $\sigma_{x,0}$, $\sigma_{y,0}$, $\sigma_{z,0}$, $\tau_{xy,0}$, $\tau_{xz,0}$ and $\tau_{yz,0}$ are the far field in-situ stress around the wellbore, MPa; P_w is the pressure of the fluid column in the wellbore, MPa; μ_k is the characteristic root of the characteristic equation corresponding to the equation of strain compatibility; a_{31}, a_{32}, and a_{33} are the elements in the flexibility coefficient matrix A. The model can be used to solve for the stress distribution around wellbore in anisotropic strata with any well deviation angle, well azimuth angle, principal stress field, stratum dip angle, etc.

The stresses around wellbore in isotropic and transverse isotropic strata are compared with the input parameters in Table 1. The former is calculated using Zhu *et al.*'s model (2013a). As can be

Table 1 Input parameters and values

Isotropic strata				Transverse isotropy			
P_w (MPa)	32	σ_z (MPa)	66	P_w (MPa)	32	σ_z (MPa)	66
∂_b (°)	0	E_h (GPa)	12	∂_b (°)	0	E_h (GPa)	36
β_b (°)	45	E_z (GPa)	12	β_b (°)	45	E_z (GPa)	12
W (°)	45	v_h	0.25	W (°)	45	v_h	0.125
σ_H (MPa)	55	v_z	0.25	σ_H (MPa)	55	v_z	0.25
σ_h (MPa)	46.2	R (m)	0.108	σ_h (MPa)	46.2	R (m)	0.108

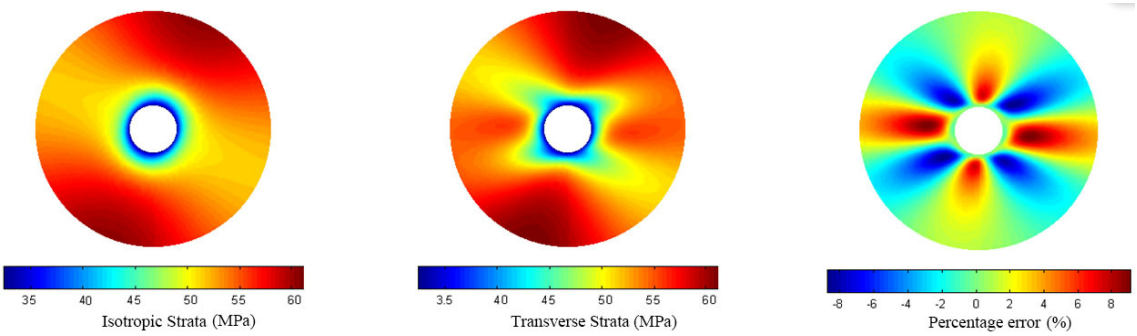

Fig. 3 Comparison of radial stresses around wellbore in isotropic and transverse isotropic strata

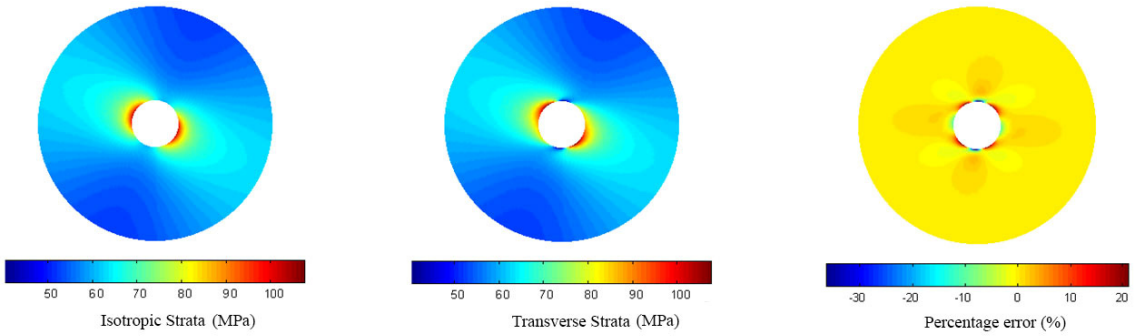

Fig. 4 Comparison of circumferential stresses around wellbore in isotropic and transverse isotropic strata

seen in Figs. 3 and 4, the mechanical anisotropy of strata, i.e., the anisotropy of stratum elasticity modulus and Poisson's ratio has a significant effect on the stresses distribution around wellbore. Thus, the isotropic model, disregarding the anisotropy of stratum elasticity modulus and Poisson's ratio, is inaccurate for the stress calculation in shale gas reservoirs.

2.3 Model of stress around perforation

For an isotropic formation, the perforation is assumed as a cylindrical micro-hole perpendicular to the borehole axis, the stresses around which can be treated as a plane problem (Fig. 5) (Zhu *et al*. 2013b). The fracture initiation pressure from Hossain's model has a relative error of less than 2%

compared with the value obtained by micro-fracture test (Hossain *et al*. 2000). The stress distribution around the perforation tunnel is expressed as (Fallahzadeh *et al*. 2010)

$$\begin{cases} \sigma'_{r'} = P \\ \sigma'_{\theta'} = \sigma_{zz} + \sigma_\theta - 2(\sigma_z - \sigma_\theta)\cos(2\theta') - 4\sigma_{\theta z}\sin(2\theta') - P \\ \sigma'_{z'} = \sigma_r - v\left[2(\sigma_z - \sigma_\theta)\cos 2\theta' + 4\sigma_{\theta z}\sin 2\theta'\right] \\ \sigma'_{r'\theta'} = 0 \\ \sigma'_{z'r'} = 0 \\ \sigma'_{\theta z'} = 2\sigma_{r\theta}\cos\theta' - 2\sigma_{rz}\sin\sin\theta' \end{cases} \tag{18}$$

where, σ_θ, $\sigma_{r\theta}$, σ_{rz}, and σ_{zz} are the components of stresses around wellbore in the cylindrical coordinate system; $\sigma'_{r'}$, $\sigma'_{\theta'}$, $\sigma'_{z'}$, $\sigma'_{r'\theta'}$, $\sigma'_{z'r'}$ and $\sigma'_{\theta'z'}$ are the stress distribution around the perforation in the cylindrical coordinate system, and θ' is the circumferential angle of the perforation.

In anisotropic reservoirs, the inclination angle between the perforation and the geodetic coordinate is $\pi/2-\alpha_b$ with the perforation angle of θ. The anisotropic flexibility coefficient matrix of the stratum $[A]$ is first transformed into the perforation coordinate system by that of the stratum $[A_b]$ in the perforation coordinate system; then the six stress components at the intersection of the perforation and wellbore are used as the original in-situ stress to calculate the stress components around the perforation. It is assumed that the stress fields of adjacent perforations do not interfere with each other. The r, θ, and z stresses on the borehole wall in anisotropic strata are assigned to the z', θ' and r' stresses in the perforation cylindrical coordinate system, respectively, and then the original in-situ stress around the perforation can be expressed as $\sigma_{r'}=\sigma_z$, $\sigma_{\theta'}=\sigma_\theta$, $\sigma_{z'}=\sigma_r$, $\sigma_{\theta'z'}=\sigma_{\theta r}$,

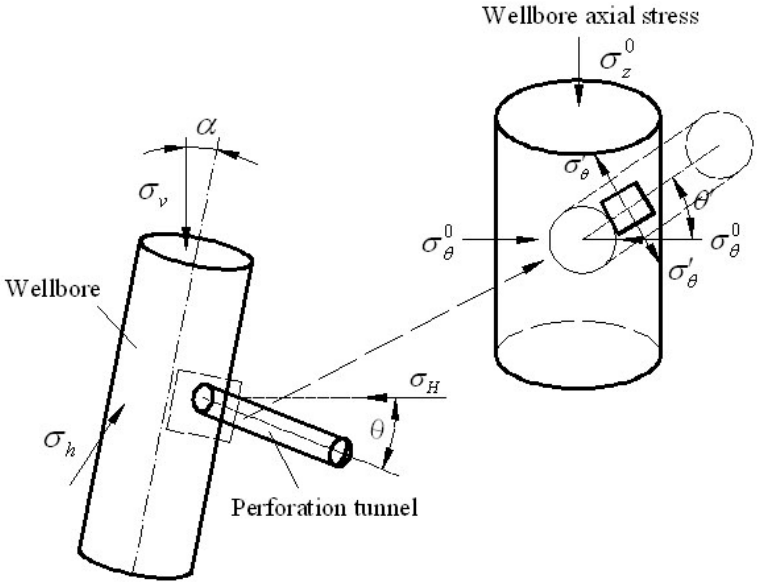

Fig. 5 Geometric model of a perforated wellbore and redistributed stress system

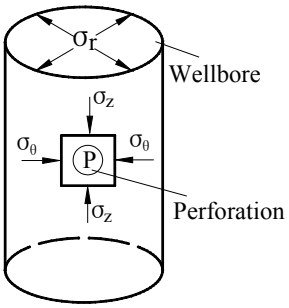

Fig. 6 Model of stresses around perforation

$\sigma_{r'z'}=\sigma_{zr}$ and $\sigma_{r'\theta'}=\sigma_{z\theta}$, shown in Fig. 6. Based on the stress field around the perforation, which is reckoned as a small open hole, the stress around it can be obtained.

2.4 Criteria for hydraulic fracture initiation pressure

Hossain *et al*. (2000) had proved that given the constant in-situ stresses, the hydraulic fracture initiation pressure based on the tensile stress criterion is more accurate than other models. The plane of fracture initiation is not exactly along the perforation axis, deviating by an angle of β. According to the LEFM theory, the hydraulic fracture initiates when the maximum principal stress in the β direction exceeds the rock tensile strength, which is (Weng 1993)

$$\sigma(\beta)=-S_t \tag{19}$$

In the previous section, stress distributions around wellbore surface and the perforation hole have been calculated. The three principal stresses around the perforation holes are

$$\begin{cases}\sigma_1'=\sigma_r' \\ \sigma_2'=\dfrac{\sigma_z'+\sigma_{\theta'}'}{2}+\sqrt{\left(\dfrac{\sigma_z'-\sigma_{\theta'}'}{2}\right)^2+\sigma_{\theta'z}'^{\,2}} \\ \sigma_3'=\dfrac{\sigma_z'+\sigma_{\theta'}'}{2}-\sqrt{\left(\dfrac{\sigma_z'-\sigma_{\theta'}'}{2}\right)^2+\sigma_{\theta'z}'^{\,2}}\end{cases} \tag{20}$$

Calculating these three stresses at any angle θ', if the formation maximum effective stress equals the rock tension strength, the hydraulic fracture initiates.

$$\sigma_3'(\theta')-\alpha P_p=-S_t \tag{21}$$

where P_p is the formation pore pressure. Angle β can be used to choose the best perforation

orientation in order to lessen the near-wellbore fracture tortuosity, consequently decreasing the risk of screening out (Fallahzadeh *et al*. 2010)

$$\beta = 0.5\tan^{-1}\left(\frac{2\sigma'_{\theta' z'}}{\sigma'_{\theta'} - \sigma'_{z'}}\right) \tag{22}$$

3. Field application

The shale gas formation in southern Sichuan Province possesses a good layered structure, with a gradual inclination of less than 5° (Fig. 7). The scanning electron microscope (SEM) image shows that the shale sample contains many micro-cracks which are unanimously oriented (Fig. 8; Yan *et al*. 2013). Under deep burial, the shale composition and structure change with significant

Fig. 7 Photo of Sichuan gas shale

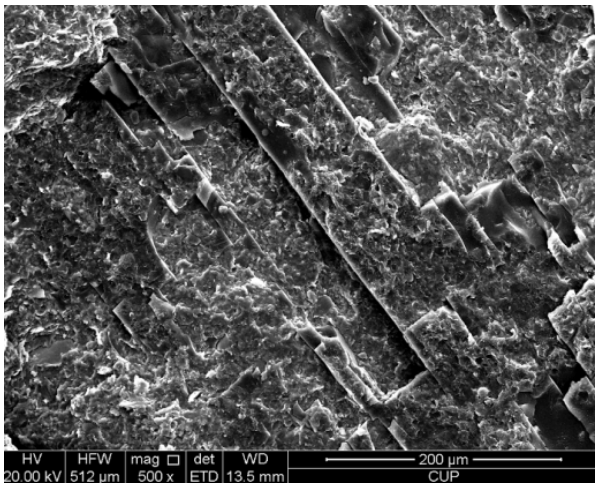

Fig. 8 SEM image of Sichuan shale

variation at the bedding planes, presenting a characteristic of transverse isotropy. The effective porosity of the reservoir is about 2%–5% and its permeability is around 200 nd.

Experiments were conducted for the core sample of the formation on the rock strength apparatus (Zhu *et al*. 2012). The experimental procedures are: (1) Core a cylindrical specimen with the diameter of 25mm and length of 50mm from the formation core sample, as shown in Fig. 9, and place it into a sealing bore after both the ends of the specimen are well ground; (2) The sealing bore containing the specimen is then put into a high-pressure autoclave, which is equipped with a data acquisition system; (3) The liquid in the high-pressure autoclave is steadily pressurized to the designed value to simulate a uniform confining pressure; (4) Afterwards, the axial strain is exerted progressively at a constant speed until the rock specimen fails. The experimental data are collected and analyzed. To study the effect of the weak bedding plane on the shale strength, different angles (Ψ) between core axis and the normal direction of bedding plane are selected, which are 0°, 15°, 30°, 45°, 60°, 75° and 90° respectively.

Shale presents significant strength anisotropy, which varies with the included angle between the direction of the maximum horizontal principal stress and the normal direction of the bedding plane. The shale strength reached the maximum when the principal stress is perpendicular to the bedding plane. While, the compressive strength reduces to the minimum when the included angle is around 50° (Fig. 10). The typical radial and axial strains of the core are depicted in Fig. 11, with

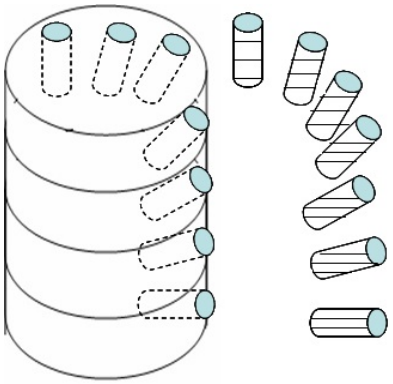

Fig. 9 Coring along different included angles with respect to the normal direction of the bedding plane

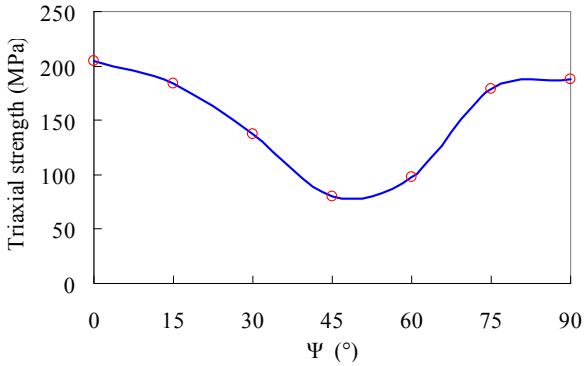

Fig. 10 Relationship between triaxial strength and the included angle Ψ

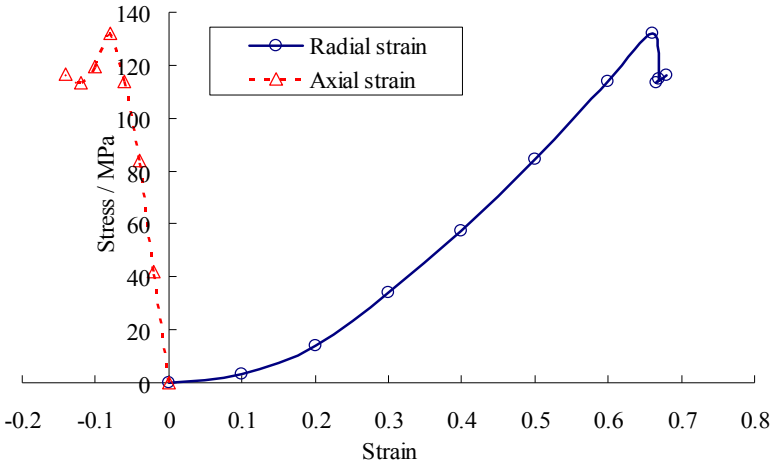

Fig. 11 Radial strain (left) and axial strain (right) of shale (Ψ = 0)

the maximum radial strain of 0.68%. The brittle failure of the core sample indicates the hard brittle characteristics of the shale gas formation. The vertical elasticity modulus of the reservoir is 30 GPa, and the transverse elasticity modulus is 33 GPa, with the same Poisson's ratio of 0.15. The uniaxial strength is 132.3 MPa and the tensile strength is 15.6 MPa.

The maximum horizontal principal stress of the reservoir is 35 MPa, the minimum is 15 MPa, the vertical stress is 21 MPa, and the pore pressure is 7.8 MPa. The wellbore diameter of a certain vertical well from the shale gas reservoir in the southern Sichuan Province is 215.9 mm; oriented perforating was performed along the direction of maximum horizontal principal stress. The perforation diameter is 16 mm and the density is 40 perforations/m. The reservoir properties are substituted into the prediction model of the fracture initiation pressure for anisotropic reservoirs. The fracture initiation pressure computed with the Matlab codes of the prediction model here is 20 MPa. Fig. 12 presents the test curves for micro-fracture test, where the actual bottom hole pressure is 20.7 MPa when fracture initiation occurred. The error between the predicted result and the measured value is only 3.5%.

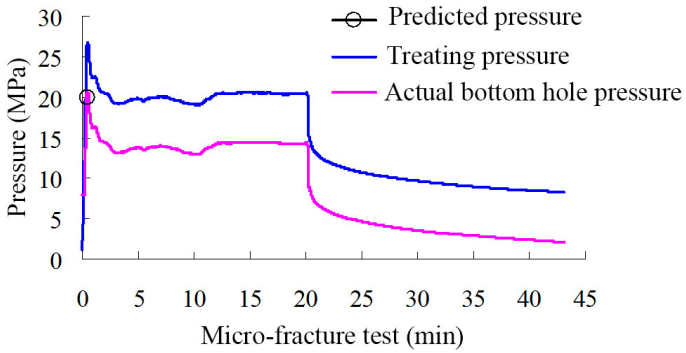

Fig. 12 Micro-fracture test curve

4. Analysis of parametric sensitivity

The anisotropy ratio k of the elasticity moduli is defined as

$$k = E_h / E_v \tag{23}$$

The anisotropy ratio k' of the Poisson's ratio is defined as

$$k' = v_h / v_v \tag{24}$$

The in-situ stress ratio n is defined as

$$n = \sigma_H / \sigma_h \tag{25}$$

Taking the shale gas reservoir in southern Sichuan Province as an example, the effects of the anisotropy of the elasticity moduli, the anisotropy of Poisson's ratio, in-situ stress ratio, perforation orientation, and tensile strength of shale on the stress distribution around the wellbore and fracture initiation pressure have been studied.

4.1 Effect of anisotropy on stress around borehole wall

It is assumed that both the well deviation angle and azimuth angle are 45°, and the stratum dip angle and strike angle are 0°. Other parameters are kept constant when the effect of a certain parameter is being studied.

As shown in Figs. 13-15, both the radial and axial stresses of the borehole wall reach the minimum when the perforation angle θ equals 0° or 180°, and the radial stress turns to be tensile. On the contrary, at the perforation angle of 90°, both of them achieve the maximum. The maximum value of the radial stress increases while the minim value decreases with the increasing anisotropy ratio of the elasticity moduli, the anisotropy ratio of Poisson's ratio, and the in-situ stress ratio. The maximum radial stresses at the anisotropy ratios of the elasticity moduli k = 2.5 and k = 1.5 are 5.1 MPa and 15.4 MPa greater than that at k = 1, respectively (Fig. 13). The anisotropy ratio of Poisson's ratio has little effect on the radial stress and a minor effect on the axial stress of the borehole wall. The maximum axial stress at k' = 1.5 is just 1.1 MPa greater than

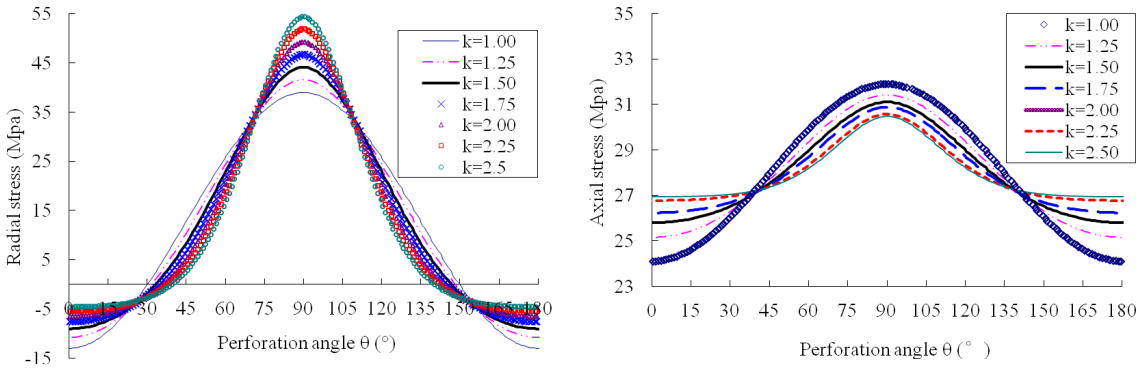

Fig. 13 Effect of the anisotropy ratio of elasticity moduli on stress around borehole wall

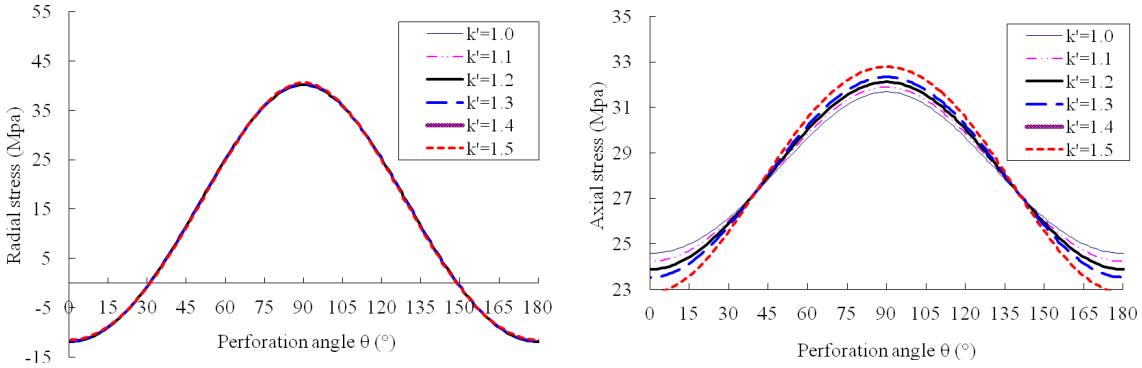

Fig. 14 Effect of anisotropy of Poisson's ratio on stresses around wellbore

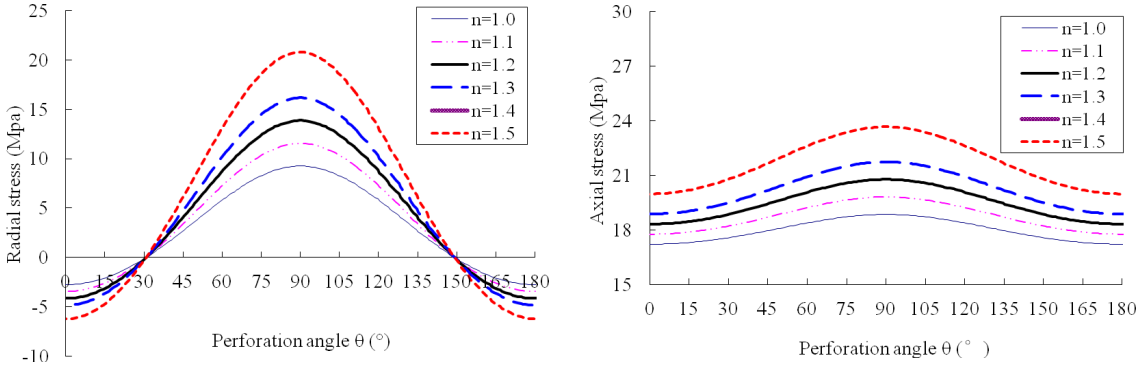

Fig. 15 Effect of principal stress ratio on stresses around wellbore

that at $k' = 1$ (Fig. 14). The maximum radial stress at the in-situ stress ratio of $n = 1.5$ is 11.6 MPa greater than that at $n = 1.5$ (Fig. 15). It is thus clear that the in-situ stress ratio has the most substantial effect on the stress of the borehole wall, followed by the anisotropy ratio of the elasticity moduli, with the anisotropy ratio of the Poisson's ratio the least.

4.2 Effect of perforation angle on fracture initiation pressure

A horizontal well drilled in the direction of the minimum horizontal principal stress is used as an example to discuss the effect of perforation angle on fracture initiation pressure. As shown in Fig. 16, at a constant anisotropy ratio of the elasticity moduli, the fracture initiation pressure increases with the perforation angle. The fracture initiation pressure reaches the minimum at the perforation angle of 0°, and attains the maximum when the perforation angle is 90°. The maximum difference between the maximum and minimum initiation pressure is 14.1 MPa with the anisotropy ratio of the elasticity moduli of 3. At the same perforation angle, the initiation pressure slightly decreases with the increasing anisotropy ratio of the elasticity moduli. The effect of the perforation angle is greater than that of the anisotropy ratio of the elasticity moduli on the fracture initiation pressure. The effect of the perforation angle in isotropic formation on the fracture initiation pressure is the same as that in the anisotropic formation. However, the effect of the

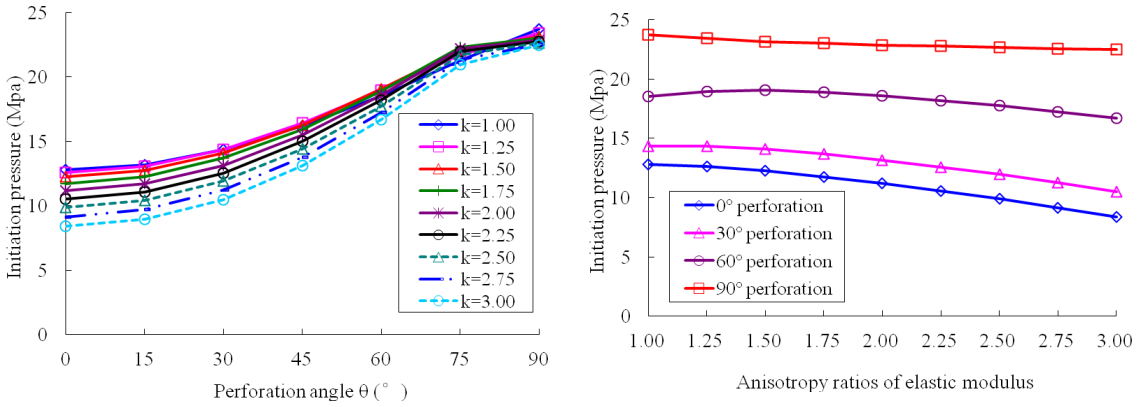

Fig. 16 Effect of perforation angle on fracture initiation pressure

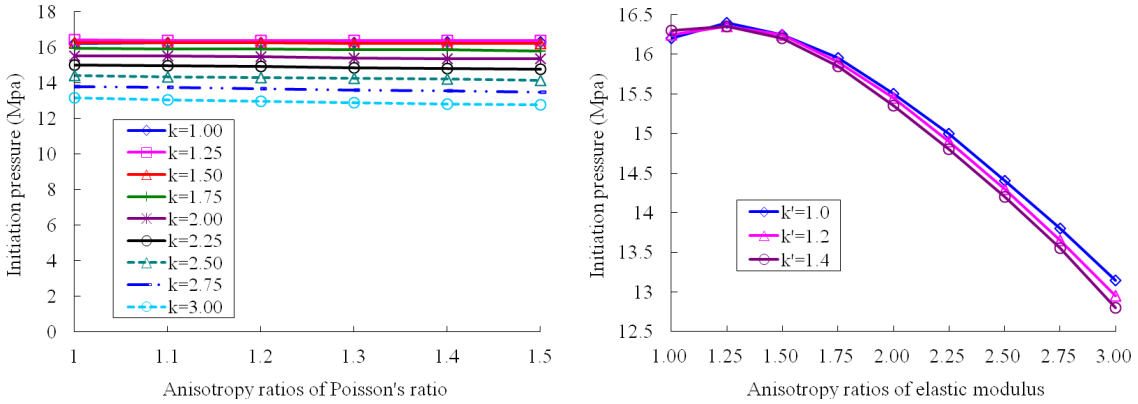

Fig. 17 Effect of the anisotropy ratio of Poisson's ratio on the fracture initiation pressure

elasticity moduli is entirely different, in that the elasticity moduli of the isotropic formation have little effect on the fracture initiation pressure.

4.3 Effect of the anisotropy ratio of poisson's ratio on the fracture initiation pressure

Oriented perforating is performed for a horizontal well drilled along the minimum horizontal principal stress, which is used for the case study here. As shown in Fig. 17, the effect of the anisotropy ratio of the Poisson's ratio on the fracture initiation pressure can be ignored, due to the fact that it is far smaller than that of the anisotropy ratio of the elasticity moduli on the fracture initiation pressure.

4.4 Effect of principal stress ratio on the fracture initiation pressure

As shown in Fig. 18, for a horizontal well drilled along the minimum primary stress direction with oriented perforation, the fracture initiation pressure increases with the increasing principal stress ratio when k is between 1.0-2.0 and n is less than 1.1. As n exceeds 1.1, the fracture initiation

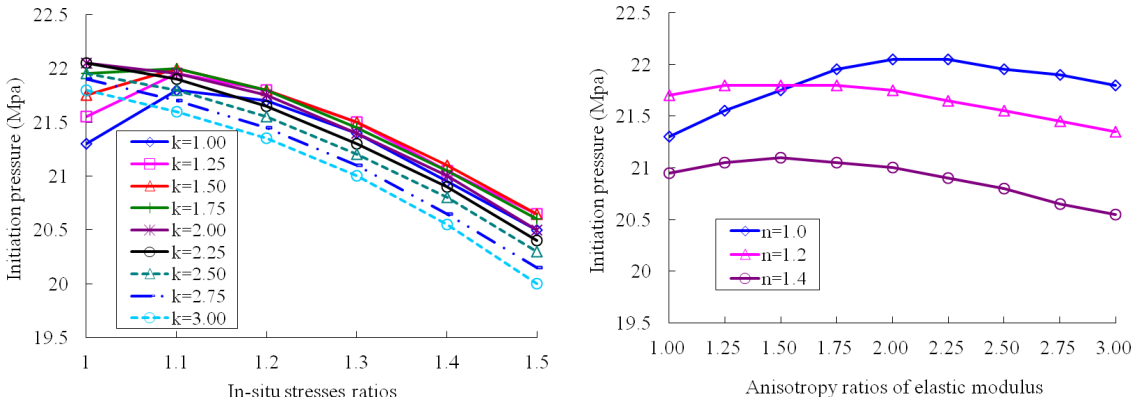

Fig. 18 Effect of principal stress ratio on the fracture initiation pressure

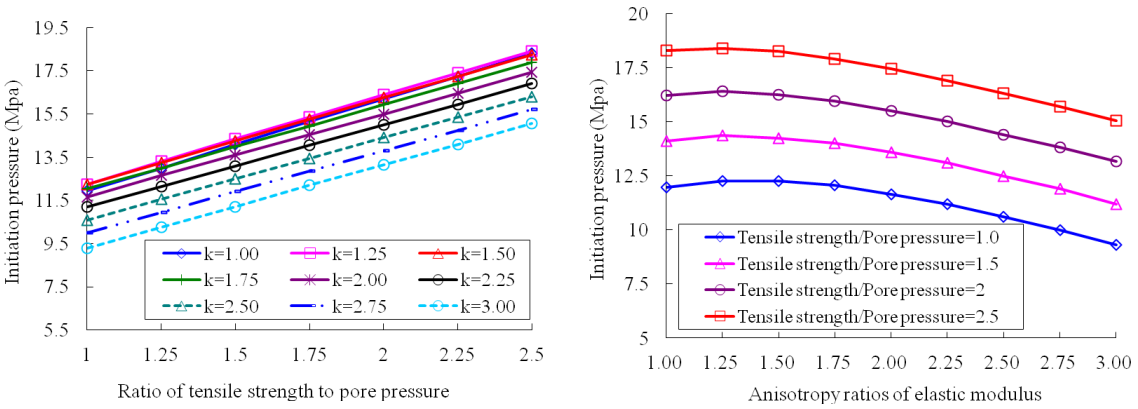

Fig. 19 Effect of ratio of tensile strength to pore pressure on fracture initiation pressure

pressure decreases with the increasing principal stress ratio. The fracture initiation pressure decreased with the increase of the in-situ stress ratio when the anisotropy ratio of the elasticity moduli is greater than 2.0. The maximum decrease of the fracture initiation pressure is 1.8 MPa when the anisotropy ratio of the elasticity moduli is 3.0. The effect of the in-situ stress ratio on the fracture initiation pressure is greater than the effect of the anisotropy ratio of the elasticity moduli on the fracture initiation pressure.

4.5 Effect of ratio of tensile strength to pore pressure on fracture initiation pressure

As shown in Fig. 19, for a horizontal well drilled along the minimum primary stress direction with oriented perforation, the fracture initiation pressure increased linearly with the increasing ratio of the tensile strength to the pore pressure. At a constant ratio, the fracture initiation pressure decreases with the increasing anisotropy ratio of the elasticity moduli. The minimum decrease of the fracture initiation pressure is approximately 2.65 MPa when the ratio is 1. Hence, the effect of the ratio of the tensile strength to the pore pressure on the fracture initiation pressure in anisotropic reservoirs cannot be ignored.

5. Conclusions

(1) The mechanical anisotropy of the formation exhibits an important effect on the stress distribution around the well in the shale gas reservoirs. Thus, the formation anisotropy should be taken into consideration while calculating the hydraulic fracture initiation pressure.
(2) On the basis of the elastic mechanics theory, a prediction model for hydraulic fracture initiation pressure in the anisotropic reservoir is established by combining the failure criterion of tensile stress. This model can be used to solve for the fracture initiation pressure with any stratum dip angle, dip direction, principal stress orientation, well deviation angle and azimuth angle. The error of the prediction result for the shale gas reservoir in the southern Sichuan Province from the measured value is only 3.5%.
(3) The fracture initiation pressure of anisotropic formation increases with the increase of the perforation angle, the ratio of the tensile strength to the pore pressure; while decreases with the increasing in-situ stress ratio and the anisotropy ratio of the elasticity moduli. The perforation angle has the largest effect on the fracture initiation pressure, followed by the in-situ stress ratio, ratio of tensile strength to pore pressure, and the anisotropy ratio of elasticity moduli as the last. The effect of the anisotropy ratio of the Poisson's ratio on the fracture initiation pressure can be neglected.

Acknowledgments

This work was supported by the SWPU Science & Technology (No. 2013XJZ003) and Academic Fund, the search Foundation of Sichuan Province under Grant No. 2014HH0004 and 14ZA0036, and the National Natural Science Foundation of China (No. 51134004 and 51374178). This work was also financially supported by 973 Program of China under Grant No. 2014CB239205.

References

Aadnøy, B.S. and høgskole, N.t. (1987), *Continuum Mechanics Analysis of the Stability of Inclined Boreholes in Anisotropic Rock Formation*, Norwegian Institute of Technology.

Amadei, B. (1983), *Rock Anisotropy and the Theory of Stress Measurements*, Lecture Notes in Engineering, Volume 2, Springer Berlin Heidelberg.

Bowker, K.A. (2003), "Recent developments of the Barnett Shale play, Fort Worth Basin", *West Texas Geological Society Bulletin*, **42**(6), 4-11.

EIA (2011), "Shale gas in the United States: Recent developments and outlook".

Fallahzadeh, S.H., Shadizadeh, S.R., Pourafshary, P. and Zare, M.R. (2010), "Modeling the perforation stress profile for analyzing hydraulic fracture initiation in a cased hole", *SPE 136990*, *The 34th Annual SPE International Conference and Exhibition*, Tinapa - Calabar, Nigeria, July-August.

Hossain, M.M., Rahrnan, M.K. and Rahman, S.S. (2000), "Hydraulic fracture initiation and propagation: Roles of wellbore trajectory, perforation and stress regimes", *J. Pet. Sci. Eng.*, **27**(3-4), 129-149.

Huang, R. and Zhuang, J. (1986), "A new prediction model of formation breakdown pressure", *Oil Drill. Prod. Tech.*, **8**(3), 1-3.

Jaeger, J.C. and Cook, N.G.W. (2007), *Fundamentals of Rock Mechanics*, (3rd Edition Ed.), Chapman and Hall, London, UK.

Khan, S., Ansari, S., Han, H. and Khosravi, N. (2011), "Importance of shale anisotropy in estimating in-situ stresses and wellbore stability analysis in Horn River basin", *SPE 149433*, *Canadian Unconventional Resources Conference*, Alberta, Canada, November.

Lekhnitskii, S.G. (1981), *Theory of Elasticity of an Anisotropic Body*, MIR Publishers, Moscow, Russia.

Mathews, L.H., Sehein, G. and Malone, M. (2007), "Stimulation of gas shales: They' re all the same – right", *SPE 106070*, *SPE Hydraulic Fracturing Technology Conference*, College Station, TX, USA, January.

Ong, S.H. (1994), "Borehole stability", Ph.D. Thesis, The University of Oklahoma, Oklahoma, OK, USA.

Ong, S.H. and Roegiers, J.C. (1995), "Fracture initiation from inclined wellbores in anisotropic formations", *J. Pet. Tech.*, **48**(7), 612-619.

Pariseau, W.G. (1968), "Plasticity theory for anisotropic rocks and soils", *The 10th U.S. Symposium on Rock Mechanics* (*USRMS*), Austin, TX, USA, May.

Prioul, R., Karpfinger, F., Deenadayalu, C. and Suarez-Rivera, R. (2011), "Improving fracture initiation predictions on arbitrarily oriented wells in anisotropic shales", *Canadian Unconventional Resources Conference*, Calgary, AB, Canada, November.

Sayers, C.M. (2005), "Seismic anisotropy of shales", *Geophys. Prospect.*, **53**(5), 667-676.

Sinha, B.K., Vissapragada, B., Renlie, L. and Tysse, S. (2006), "Radial profiling of the three formation shear moduli and its application to well completions", *Geophys.*, **71**(6), 65-77.

Suarez-Rivera, R., Green, S.J., McLennan, J. and Bai, M. (2006), "Effect of layered heterogeneity on fracture initiation in tight gas shales", *SPE 103327*, *SPE Annual Technical Conference and Exhibition*, San Antonio, TX, USA, September.

Suarez-Rivera, R., Deenadayalu, C. and Yang, Y. (2009), "SS: Unlocking the unconventional oil and gas reservoirs: The effect of laminated heterogeneity in wellbore stability and completion of tight gas shale reservoirs", *OTC 20269*, *Offshore Technology Conference*, Houston, TX, USA, May.

Thiercelin, M. and Plumb, R. (1994), "A core-based prediction of lithologic stress contrasts in East Texas formations", *SPE Formation Eval.*, **9**(4), 251-258.

Walsh, J., Sinha, B., Plona, T., Miller, D., Bentley, D. and Ammerman, M. (2007), "Derivation of anisotropy parameters in a shale using borehole sonic data", *SEG Technical Program Expanded Abstracts*, **1**(26), 323-327.

Wang, Y. and Li, Z. (1999), "A study of in-situ stresses in transversely isotropic formations", ACTA PETROL EI SINICA, **20**(1), 34-37.

Weng, X. (1993), "Fracture initiation and propagation from deviated wellbores", *SPE 26597*, *The 68th Annual Technical Conference and Exhibition of the Society of Petroleum Engineers*, Houston, TX, USA, October.

Yan, C.L., Deng, J.G., Yu, B.H., Tan, Q., Deng, F.C., Zhu, H.Y., Hu, L.B. and Chen, Z.J. (2013), "Research on collapsing pressure of gas shale", *Chinese J. Rock Mech. Eng.*, **32**(8), 1595-1602.

Zhu, H.Y., Deng, J.G., Xie, Y.H., Huang, K.W., Zhao, J.Y. and Yu, B.H. (2012), "Rock mechanics characteristic of complex formation and faster drilling techniques in Western South China Sea oilfields", *Ocean Eng.*, **44**, 33-45.

Zhu, H.Y., Deng, J.G., Chen, Z.J., An, F.C., Liu, S.J., Peng, C.Y., Wen, M. and Dong, G. (2013a), "Perforation optimization of hydraulic fracturing of oil and gas well", *Geomech. Eng., Int. J.*, **5**(5), 463-483.

Zhu, H.Y., Deng, J.G., Li, S.Y., Chen, Z.R. and Yan, W. (2013b), "Numerical simulation and laboratory experiments of hydraulic fracturing of highly deviated well", *Appl. Mech. Mater.*, **275-277**, 278-281.

CC

Appendix

Based on the solutions to the anisotropic plane problem provided by Lekhnitskii (1981), Amadei (1983), Aadnoy (1987) and Ong (1994), the stress distribution model around the wellbore in anisotropic formations have been established. As shown in Fig. A1, the following assumptions are made:

① The formation is considered as a linear elastic, continuous, and homogeneous anisotropic body, which needs 21 elastic parameters for the mathematical description. In case that not all of these parameters can be obtained, this model is simplified as orthotropic or transverse isotropic body.

② The length of the wellbore is assumed as infinite, along which the strain is zero, i.e., the stress distribution around the wellbore in the anisotropic formation is approximated as a plane strain problem.

(1) Governing equation

Neglecting the gravity, the stress in the wellbore coordinates should satisfy the equilibrium differential equation

$$\begin{cases} \dfrac{\partial \sigma_x}{\partial x} + \dfrac{\partial \tau_{yx}}{\partial y} + \dfrac{\partial \tau_{xz}}{\partial z} = 0 \\ \dfrac{\partial \tau_{xy}}{\partial x} + \dfrac{\partial \sigma_y}{\partial y} + \dfrac{\partial \tau_{yz}}{\partial z} = 0 \\ \dfrac{\partial \tau_{xz}}{\partial x} + \dfrac{\partial \tau_{yz}}{\partial y} + \dfrac{\partial \sigma_z}{\partial z} = 0 \end{cases} \tag{A.1}$$

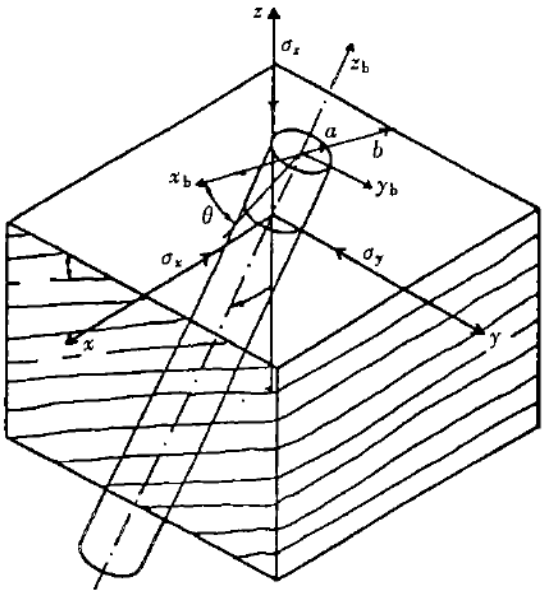

Fig. A1 Wellbore coordinates of anisotropic formation

Applying the generalized Hook's law, the constitutive equation for the anisotropic equation is

$$\begin{pmatrix} \varepsilon_{xx} \\ \varepsilon_{yy} \\ \varepsilon_{zz} \\ \gamma_{yz} \\ \gamma_{zx} \\ \gamma_{xy} \end{pmatrix} = \begin{pmatrix} a_{11} & a_{12} & a_{13} & a_{14} & a_{15} & a_{16} \\ a_{21} & a_{22} & a_{23} & a_{24} & a_{25} & a_{26} \\ a_{31} & a_{32} & a_{33} & a_{34} & a_{35} & a_{36} \\ a_{41} & a_{42} & a_{43} & a_{44} & a_{45} & a_{46} \\ a_{51} & a_{52} & a_{53} & a_{54} & a_{55} & a_{56} \\ a_{61} & a_{62} & a_{63} & a_{64} & a_{65} & a_{66} \end{pmatrix} \begin{pmatrix} \sigma_x \\ \sigma_y \\ \sigma_z \\ \tau_{yz} \\ \tau_{zx} \\ \tau_{xy} \end{pmatrix} \tag{A.2}$$

If it is written in the matrix form, we have

$$\{\varepsilon\} = [A]\{\sigma\} \tag{A.3}$$

where, strain tensor $\{\varepsilon\} = \{\varepsilon_x \quad \varepsilon_y \quad \varepsilon_z \quad \varepsilon_{yz} \quad \varepsilon_{xz} \quad \varepsilon_{xy}\}^T$; $[A]$ is the flexibility coefficient matrix for anisotropic formation, $[A] = a_{ij}$ $(i, j = 1\sim6)$; the stress tensor $\{\sigma\} = \{\sigma_x \quad \sigma_y \quad \sigma_z \quad \sigma_{yz} \quad \sigma_{xz} \quad \sigma_{xy}\}^T$.

Based on the plain strain conditions and the constitutive equation, as $\varepsilon_z = 0$, σ_z can be expressed with

$$\sigma_z = -\frac{1}{a_{33}}(a_{31}\sigma_x + a_{32}\sigma_y + a_{34}\tau_{yz} + a_{35}\tau_{xz} + a_{36}\tau_{xy}) \tag{A.4}$$

In the generalized plane strain theory, strain components are independent of z. Thus, the consistency equations are

$$\begin{cases} \dfrac{\partial^2 \varepsilon_x}{\partial y^2} + \dfrac{\partial^2 \varepsilon_y}{\partial x^2} = \dfrac{\partial^2 \gamma_{xy}}{\partial x \partial y} \\ \dfrac{\partial \gamma_{xz}}{\partial y} - \dfrac{\partial \gamma_{yz}}{\partial x} = 0 \\ \dfrac{\partial^2 \varepsilon_z}{\partial y^2} = \dfrac{\partial^2 \varepsilon_z}{\partial x^2} = \dfrac{\partial^2 \varepsilon_z}{\partial x \partial y} = 0 \end{cases} \tag{A.5}$$

(2) General solution to the plain strain problem of anisotropic formation

There exist functions $F(x, y)$ and $\psi(x, y)$ satisfying

$$\sigma_x = \frac{\partial^2 F}{\partial y^2}, \quad \sigma_y = \frac{\partial^2 F}{\partial x^2}, \quad \tau_{xy} = -\frac{\partial^2 F}{\partial x \partial y}, \quad \tau_{xz} = \frac{\partial \psi}{\partial y}, \quad \tau_{xz} = -\frac{\partial \psi}{\partial x} \tag{A.6}$$

First substituting Eqs. (A.3) and (A.4) into Eq. (A.6), and then taking the results into the consistency Eq. (A.5), the Beltrami-Michell equation can be obtained

$$\begin{cases} L_4 F + L_3 \psi = 0 \\ L_3 F + L_2 \psi = 0 \end{cases} \tag{A.7}$$

where L_2, L_3 and L_4 are the second order, third order and fourth order differential operators, as are denoted by

$$\begin{cases} L_2 = \beta_{44}\dfrac{\partial^2}{\partial x^2} - 2\beta_{45}\dfrac{\partial^2}{\partial x \partial y} + \beta_{55}\dfrac{\partial^2}{\partial y^2} \\ L_3 = -\beta_{24}\dfrac{\partial^3}{\partial x^3} + (\beta_{25} + \beta_{46})\dfrac{\partial^3}{\partial x^2 \partial y} - (\beta_{14} + \beta_{56})\dfrac{\partial^3}{\partial x \partial y^2} + \beta_{15}\dfrac{\partial^3}{\partial y^3} \\ L_4 = \beta_{22}\dfrac{\partial^4}{\partial x^4} - 2\beta_{26}\dfrac{\partial^4}{\partial x^3 \partial y} + (2\beta_{12} + \beta_{66})\dfrac{\partial^4}{\partial x^2 \partial y^2} - 2\beta_{16}\dfrac{\partial^4}{\partial x \partial y^3} + \beta_{11}\dfrac{\partial^4}{\partial y^4} \end{cases} \tag{A.8}$$

where β_{ij} is the reduced tensor of strain coefficient

$$\beta_{ij} = a_{ij} - \frac{a_{i3}a_{j3}}{a_{33}} \qquad (i, j = 1, 2, 4, 5, 6) \tag{A.9}$$

Solving Eq. (A.53), a sixth order differential equation is attained

$$(L_4 L_2 - L_3^2)F = 0 \tag{A.10}$$

The characteristic equation corresponding to Eq. (A.56) is

$$I_4(\mu) I_2(\mu) - I_3^2(\mu) = 0 \tag{A.11}$$

where

$$\begin{cases} I_2(\mu) = \beta_{55}\mu^2 - 2\beta_{45}\mu + \beta_{44} \\ I_3(\mu) = \beta_{15}\mu^3 - (\beta_{14} + \beta_{56})\mu^2 + (\beta_{25} + \beta_{46})\mu - \beta_{24} \\ I_4(\mu) = \beta_{11}\mu^4 - 2\beta_{16}\mu^3 + (2\beta_{12} + \beta_{66})\mu^2 - 2\beta_{26}\mu + \beta_{22} \end{cases} \tag{A.12}$$

There are six characteristic roots for Eq. (A.11) μ_k (k = 1~6); μ_1, μ_2 and μ_3 are the three of them, while μ_1^*, μ_2^* and μ_3^* are the corresponding conjugate roots. λ_1, λ_2 and λ_3 are defined as

$$\lambda_1 = -\frac{I_3(\mu_1)}{I_2(\mu_1)}, \quad \lambda_2 = -\frac{I_3(\mu_2)}{I_2(\mu_2)}, \quad \lambda_3 = -\frac{I_3(\mu_3)}{I_4(\mu_3)} \tag{A.13}$$

Lekhnitskii (1981) presented the general expressions for $F(x, y)$ and $\psi(x, y)$

$$\begin{cases} F = 2\,\mathrm{Re}\{F_1(z_1) + F_2(z_2) + F_3(z_3)\} \\ \psi = 2\,\mathrm{Re}\{\lambda_1 F_1'(z_1) + \lambda_2 F_2'(z_2) + F_3'(z_3)/\lambda_3\} \end{cases} \tag{A.14}$$

where Re is the real part of the expression in the braces; $F(z_k)(k = 1, 2, 3)$ is the function of the complex variable, $z_k = x + \mu_k y$; x and y are the coordinates of the stress, strain, and displacement to be solved. Meanwhile, Lekhnitskii defined three analytical functions ϕ_k of z_k

$$\phi_1(z_1) = F_1'(z_1), \quad \phi_2(z_2) = F_2'(z_2), \quad \phi_3(z_3) = F_3'(z_3)/\lambda_3 \tag{A.15}$$

Combining Eqs. (A.5), (A.13) and (A.14), the expressions for stress components around the wellbore are

$$\begin{cases} \sigma_{x,h} = 2\,\mathrm{Re}\{\mu_1^2\phi_1'(z_1) + \mu_2^2\phi_2'(z_2) + \lambda_3\mu_3^2\phi_3'(z_3)\} \\ \sigma_{y,h} = 2\,\mathrm{Re}\{\phi_1'(z_1) + \phi_2'(z_2) + \lambda_3\phi_3'(z_3)\} \\ \tau_{xy,h} = -2\,\mathrm{Re}\{\mu_1\phi_1'(z_1) + \mu_2\phi_2'(z_2) + \lambda_3\mu_3\phi_3'(z_3)\} \\ \tau_{xz,h} = 2\,\mathrm{Re}\{\lambda_1\mu_1\phi_1'(z_1) + \lambda_2\mu_2\phi_2'(z_2) + \mu_3\phi_3'(z_3)\} \\ \tau_{yz,h} = -2\,\mathrm{Re}\{\lambda_1\phi_1'(z_1) + \lambda_2\phi_2'(z_2) + \phi_3'(z_3)\} \\ \sigma_{z,h} = -(a_{31}\sigma_{x,h} + a_{32}\sigma_{y,h} + a_{34}\tau_{yz,h} + a_{35}\tau_{xz,h} + a_{36}\tau_{xy,h})/a_{33} \end{cases} \tag{A.16}$$

where $\sigma_{x,h}$, $\sigma_{y,h}$, $\sigma_{z,h}$, $\tau_{xy,h}$, $\tau_{xz,h}$ and $\tau_{yz,h}$ are the stress components induced by the boundary conditions of the borehole and borehole wall.

(3) Analytical model of stress around wellbore in anisotropic formation

The boundary condition on the borehole wall is

$$\begin{cases} -\sigma_x \dfrac{dy}{ds} + \tau_{xy} \dfrac{dx}{ds} = \xi_x \\ -\tau_{xy} \dfrac{dy}{ds} + \sigma_y \dfrac{dx}{ds} = \xi_y \\ -\tau_{xz} \dfrac{dy}{ds} + \tau_{yz} \dfrac{dx}{ds} = \xi_z \end{cases} \tag{A.17}$$

where ξ_x, ξ_y and ξ_z are external stress components in the x, y and z directions exerted on the borehole wall. Substituting Eq. (A.5) into Eq. (A.17), the boundary condition can be written as

$$\begin{cases} \dfrac{\partial}{\partial y}\left(\dfrac{\partial F}{\partial y}\right)\dfrac{dy}{ds}+\dfrac{\partial}{\partial x}\left(\dfrac{\partial F}{\partial y}\right)\dfrac{dx}{ds}=-\xi_x \\ \dfrac{\partial}{\partial y}\left(\dfrac{\partial F}{\partial x}\right)\dfrac{dy}{ds}+\dfrac{\partial}{\partial x}\left(\dfrac{\partial F}{\partial x}\right)\dfrac{dx}{ds}=\xi_y \\ \dfrac{\partial \psi}{\partial y}\dfrac{dy}{ds}+\dfrac{\partial \psi}{\partial x}\dfrac{dx}{ds}=-\xi_z \end{cases} \tag{A.18}$$

Integrating Eq. (A.18) from $S = 0$ gives

$$\begin{cases} \dfrac{\partial F}{\partial y}=\displaystyle\int_0^s -\xi_x ds + C_1 \\ \dfrac{\partial F}{\partial x}=\displaystyle\int_0^s -\xi_y ds + C_2 \\ \psi=\displaystyle\int_0^s -\xi_z ds + C_3 \end{cases} \tag{A.19}$$

By differentiating Eq. (A.19), the combination of Eqs. (A.15) and (A.19) yields

$$\begin{cases} \dfrac{\partial F}{\partial y}=2\,\mathrm{Re}\{\mu_1\varphi_1(z_1)+\mu_2\varphi_2(z_2)+\lambda_3\mu_3\varphi_3(z_3)\}=-\displaystyle\int_0^s \xi_x ds \\ \dfrac{\partial F}{\partial x}=2\,\mathrm{Re}\{\varphi_1(z_1)+\varphi_2(z_2)+\lambda_3\varphi_3(z_3)\}=-\displaystyle\int_0^s \xi_y ds \\ \psi=2\,\mathrm{Re}\{\lambda_1\varphi_1(z_1)+\lambda_2\varphi_2(z_2)+\varphi_3(z_3)\}=-\displaystyle\int_0^s \xi_z ds \end{cases} \tag{A.20}$$

Substituting Eq. (A.20) into Eq. (A.14), the stress distribution around the wellbore in anisotropic formation can be achieved. For the plane strain problem, the boundary conditions generated from in-situ stress field $\sigma_{ij,0}$ ($i, j = x, y, z$) on the borehole wall are

$$\begin{cases} \xi_{x,0}=\sigma_{x,0}\cos(\vec{n},x)+\tau_{xy,0}\cos(\vec{n},y) \\ \xi_{y,0}=\tau_{xy,0}\cos(\vec{n},x)+\sigma_{y,0}\cos(\vec{n},y) \\ \xi_{z,0}=\tau_{zx,0}\cos(\vec{n},x)+\tau_{zy,0}\cos(\vec{n},y) \end{cases} \tag{A.21}$$

$$\begin{cases} \cos(\vec{n},x)=-dy/ds \\ \cos(\vec{n},y)=dx/ds \end{cases} \tag{A.22}$$

$$x=R\cos\theta,\quad y=R\sin\theta,\quad ds=Rd\theta \tag{A.23}$$

where r is the borehole radius. Substituting Eqs. (A.22) and (A.23) into Eq. (A.21) yields

$$\begin{cases} \xi_{x,0} = -\sigma_{x,0}\cos\theta - \tau_{xy,0}\sin\theta \\ \xi_{y,0} = -\tau_{xy,0}\cos\theta - \sigma_{y,0}\sin\theta \\ \xi_{z,0} = -\tau_{zx,0}\cos\theta - \tau_{zy,0}\sin\theta \end{cases} \tag{A.24}$$

Similarly, the boundary conditions induced by the drilling fluid column are: $\sigma_{x,0} = \sigma_{y,0} = p_w$, and $\tau_{xy,0} = \tau_{yz,0} = \tau_{xz,0} = 0$

$$\xi_{x,w} = -p_w\cos\theta, \quad \xi_{y,w} = -p_w\sin\theta, \quad \xi_{z,w} = 0 \tag{A.25}$$

Since the boundary conditions generated from in-situ stress field $\sigma_{ij,0}$ ($i, j = x, y, z$) are opposite to the wellbore coordinate directions, thus they should be transformed by multiplying -1. Then the boundary conditions induced by the in-situ stress and drilling fluid column can be expressed as

$$\begin{cases} \xi_x = (\sigma_{x,0} - p_w)\cos\theta + \tau_{xy,0}\sin\theta \\ \xi_y = \tau_{xy,0}\cos\theta + (\sigma_{y,0} - p_w)\sin\theta \\ \xi_z = \tau_{zx,0}\cos\theta + \tau_{zy,0}\sin\theta \end{cases} \tag{A.26}$$

Substituting Eq. (A.26) into Eq. (A.20) and applying the Fourier series expansion

$$\begin{cases} 2\,\mathrm{Re}\{\mu_1\phi_1(z_1) + \mu_2\phi_2(z_2) + \lambda_3\mu_3\phi_3(z_3)\} = \sum_1^{\infty}(a_m e^{im\theta} + \bar{a}_m e^{-im\theta}) = \sum_{m=1}^{\infty}(2\,\mathrm{Re}\,\bar{a}_m e^{-im\theta}) \\ 2\,\mathrm{Re}\{\phi_1(z_1) + \phi_2(z_2) + \lambda_3\phi_3(z_3)\} = \sum_1^{\infty}(b_m e^{im\theta} + \bar{b}_m e^{-im\theta}) = \sum_{m=1}^{\infty}(2\,\mathrm{Re}\,\bar{b}_m e^{-im\theta}) \\ 2\,\mathrm{Re}\{\lambda_1\phi_1(z_1) + \lambda_2\phi_2(z_2) + \phi_3(z_3)\} = \sum_1^{\infty}(c_m e^{im\theta} + \bar{c}_m e^{-im\theta}) = \sum_{m=1}^{\infty}(2\,\mathrm{Re}\,\bar{c}_m e^{-im\theta}) \end{cases} \tag{A.27}$$

and

$$\begin{cases} \bar{a}_1 = R[i\tau_{xy,0} - (\sigma_{y,0} - p_w)]/2 \\ \bar{b}_1 = R[\tau_{xy,0} - i(\sigma_{x,0} - p_w)]/2 \\ \bar{c}_1 = R(\tau_{yz,0} - i\tau_{xz,0})/2 \\ \bar{a}_m = \bar{b}_m = \bar{c}_m = 0, \quad m \geq 2 \end{cases} \tag{A.28}$$

Lekhnitskii (1981) put forward the expression for conformal transformation

$$\frac{z_k}{R}=\frac{1-i\mu_k}{2}\eta_k+\frac{1+i\mu_k}{2}\frac{1}{\eta_k},\quad k=1,2,3 \tag{A.29}$$

$$z_k=x+\mu_k y,\quad k=1,2,3 \tag{A.30}$$

where x and y is the coordinates of the stress point to be solved. It is known that

$$\eta_k=\frac{\frac{z_k}{R}+\sqrt{\left(\frac{z_k}{R}\right)^2-1-\mu_k^2}}{1-i\mu_k} \tag{A.31}$$

On the borehole wall

$$z_k=R(\cos\theta+\mu_k\sin\theta),\quad \eta_k=e^{i\theta},\quad k=1,2,3 \tag{A.32}$$

Assuming that

$$\phi_k(z_k)=\sum_{m=1}^{\infty}A_{km}\eta_k^{-m},\quad k=1,2,3 \tag{A.33}$$

Substituting Eqs. (A.28)~(A.33) into Eq. (A.27), we have

$$\begin{cases}\phi_1(z_1)=\dfrac{1}{\Delta}\displaystyle\sum_{m=1}^{\infty}\left[(\mu_2-\lambda_2\lambda_3\mu_3)\bar{a}_m+(\lambda_2\lambda_3-1)\bar{b}_m+\lambda_3(\mu_3-\mu_2)\bar{c}_m\right]\eta_1^{-m}\\ \phi_2(z_2)=\dfrac{1}{\Delta}\displaystyle\sum_{m=1}^{\infty}\left[(\lambda_1\lambda_3\mu_3-\mu_1)\bar{a}_m+(1-\lambda_1\lambda_3)\bar{b}_m+\lambda_3(\mu_1-\mu_3)\bar{c}_m\right]\eta_2^{-m}\\ \phi_3(z_3)=\dfrac{1}{\Delta}\displaystyle\sum_{m=1}^{\infty}\left[(\mu_1\lambda_2-\mu_2\lambda_1)\bar{a}_m+(\lambda_1-\lambda_2)\bar{b}_m+\lambda_3(\mu_2-\mu_1)\bar{c}_m\right]\eta_3^{-m}\end{cases} \tag{A.34}$$

where

$$\Delta=\mu_2-\mu_1+\lambda_2\lambda_3(\mu_1-\mu_3)+\lambda_1\lambda_3(\mu_3-\mu_2) \tag{A.35}$$

Differentiating Eq. (A.35) and combining Eq. (A.28) with Eq. (A.31) gives

$$\begin{cases} \phi_1'(z_1) = -\dfrac{1}{\Delta R\eta_1\sqrt{\left(\dfrac{z_1}{R}\right)^2 - 1 - \mu_1^2}}\left[\overline{a}_1(\mu_2 - \lambda_2\lambda_3\mu_3) + \overline{b}_1(\lambda_2\lambda_3 - 1) + \overline{c}_1\lambda_3(\mu_3 - \mu_2)\right] \\ \phi_2'(z_2) = -\dfrac{1}{\Delta R\eta_2\sqrt{\left(\dfrac{z_2}{R}\right)^2 - 1 - \mu_2^2}}\left[\overline{a}_1(\lambda_1\lambda_3\mu_3 - \mu_1) + \overline{b}_1(1 - \lambda_1\lambda_3) + \overline{c}_1\lambda_3(\mu_1 - \mu_3)\right] \\ \phi_3'(z_3) = -\dfrac{1}{\Delta R\eta_3\sqrt{\left(\dfrac{z_3}{R}\right)^2 - 1 - \mu_3^2}}\left[\overline{a}_1(\mu_1\lambda_2 - \mu_2\lambda_1) + \overline{b}_1(\lambda_1 - \lambda_2) + \overline{c}_1(\mu_2 - \mu_1)\right] \end{cases} \tag{A.36}$$

i.e.,

$$\begin{cases} \phi_1'(z_1) = -\dfrac{1}{2\Delta\eta_1\sqrt{\left(\dfrac{z_1}{R}\right)^2 - 1 - \mu_1^2}}\Big[(i\tau_{xy,0} - \sigma_{y,0} + p_w)(\mu_2 - \lambda_2\lambda_3\mu_3) \\ \qquad + (\tau_{xy,0} - i\sigma_{x,0} + ip_w)(\lambda_2\lambda_3 - 1) + \lambda_3(\tau_{yz,0} - i\tau_{xz,0})(\mu_3 - \mu_2)\Big] \\ \phi_2'(z_2) = -\dfrac{1}{2\Delta\eta_2\sqrt{\left(\dfrac{z_2}{R}\right)^2 - 1 - \mu_2^2}}\Big[(i\tau_{xy,0} - \sigma_{y,0} + p_w)(\lambda_1\lambda_3\mu_3 - \mu_1) \\ \qquad + (\tau_{xy,0} - i\sigma_{x,0} + ip_w)(1 - \lambda_1\lambda_3) + (\tau_{yz,0} - i\tau_{xz,0})\lambda_3(\mu_1 - \mu_3)\Big] \\ \phi_3'(z_3) = -\dfrac{1}{2\Delta\eta_3\sqrt{\left(\dfrac{z_3}{R}\right)^2 - 1 - \mu_3^2}}\Big[(i\tau_{xy,0} - \sigma_{y,0} + p_w)(\mu_1\lambda_2 - \mu_2\lambda_1) \\ \qquad + (\tau_{xy,0} - i\sigma_{x,0} + ip_w)(\lambda_1 - \lambda_2) + (\tau_{yz,0} - i\tau_{xz,0})(\mu_2 - \mu_1)\Big] \end{cases} \tag{A.37}$$

Therefore, the circumferential stress can be calculated by superposing the stresses induced from far field in-situ stress and the boundary conditions of both the wellbore and borehole wall, with the following equation

$$\begin{cases} \sigma_x = \sigma_{x,0} + \sigma_{x,h} = \sigma_{x,0} + 2\,\mathrm{Re}\left\{\mu_1^2\phi_1'(z_1) + \mu_2^2\phi_2'(z_2) + \lambda_3\mu_3^2\phi_3'(z_3)\right\} \\ \sigma_y = \sigma_{y,0} + \sigma_{y,h} = \sigma_{y,0} + 2\,\mathrm{Re}\left\{\phi_1'(z_1) + \phi_2'(z_2) + \lambda_3\phi_3'(z_3)\right\} \\ \tau_{xy} = \tau_{xy,0} + \tau_{xy,h} = \tau_{xy,0} - 2\,\mathrm{Re}\left\{\mu_1\phi_1'(z_1) + \mu_2\phi_2'(z_2) + \lambda_3\mu_3\phi_3'(z_3)\right\} \\ \tau_{xz} = \tau_{xz,0} + \tau_{xz,h} = \tau_{xz,0} + 2\,\mathrm{Re}\left\{\lambda_1\mu_1\phi_1'(z_1) + \lambda_2\mu_2\phi_2'(z_2) + \mu_3\phi_3'(z_3)\right\} \\ \tau_{yz} = \tau_{yz,0} + \tau_{yz,h} = \tau_{yz,0} - 2\,\mathrm{Re}\left\{\lambda_1\phi_1'(z_1) + \lambda_2\phi_2'(z_2) + \phi_3'(z_3)\right\} \\ \sigma_z = \sigma_{z,0} + \sigma_{z,h} = \sigma_{z,0} - \left(a_{31}\sigma_{x,h} + a_{32}\sigma_{y,h} + a_{34}\tau_{yz,h} + a_{35}\tau_{xz,h} + a_{36}\tau_{xy,h}\right) \Big/ a_{33} \end{cases} \tag{A.38}$$

This model can be used to solve the fracture initiation pressure problems with any wellbore deviation and azimuth, in-situ stress field, stratum dip angle, and dip direction in anisotropic formations.